Research Article

Visible Light-driven BiOI/ZnO Photocatalyst Films and Its Photodegradation of Methomyl Insecticide

Natkritta Boonprakob*
Department of Chemistry, Faculty of Science and Technology, Uttaradit Rajabhat University, Uttaradit, Thailand

Duangdao Channei
Department of Chemistry, Faculty of Science, Naresuan University, Phitsanulok, Thailand

Burapat Inceesungvorn
Department of Chemistry, Faculty of Science, Chiang Mai University, Chiang Mai, Thailand

Chen Zhao
School of Materials and Energy, Guangdong University of Technology, Guangzhou, P.R. China

* Corresponding author. E-mail: nboonprakob@gmail.com DOI: 10.14416/j.ijast.2018.08.003
Received: 11 June 2018; Accepted: 15 August 2018; Published online: 28 August 2018

Abstract
Bismuth oxyiodide/zinc oxide (BiOI/ZnO) composite photocatalyst films were successfully prepared by a simple low temperature co-precipitation method coupled with a reflux procedure. Mole ratios of BiOI and ZnO were varied from 0, 0.125, 0.25 and 0.50 mol% while X-ray diffraction patterns confirmed characteristic peaks of BiOI and ZnO in all composite samples. Optimal photocatalytic efficiency of methomyl photodegradation under visible light irradiation was recorded for 0.25 mol% BiOI/ZnO photocatalyst at 58%. Increase in BiOI content resulted in higher photocatalytic activity than for pure ZnO and commercial ZnO. Optimal heterojunction content at 0.25 mol% BiOI/ZnO was recorded between hexagonal wurtzite ZnO and tetragonal BiOI, with high crystalline particles leading to enhanced specific surface light absorption capacity in the visible region. Based on these good characterization results for interfacial surface and X-ray Photoelectron Spectroscopy (XPS), the combination of both semiconductors generated more electrons, resulting in enhanced photocatalytic performance of methomyl degradation under visible light irradiation.

Keywords: BiOI, ZnO, Photocatalyst film, Composite materials

1 Introduction

Methomyl is a carbamate insecticide which is used in agricultural areas at high volumes in Thailand [1], thereby contaminating soil and water. Many reports have examined photocatalysis applications for treating insecticide-contaminated wastewater [2]–[4]. Zinc oxide (ZnO) semiconductors have attracted increased interest in applications of photocatalysis, gas sensors, solar cells, and supercapacitors because of their promising properties such as low cost, physical and chemical stability, and easy preparation. However, performance of intrinsic ZnO semiconductors is limited by several factors including insufficient light absorption, poor charge transport and low conductivity [5]. Furthermore, the wide band gap of ZnO (3.37 eV)

Please cite this article as: N. Boonprakob, D. Channei, B. Inceesungvorn, and C. Zhao, "Visible light-driven BiOI/ZnO photocatalyst films and its photodegradation of methomyl insecticide," *KMUTNB Int J Appl Sci Technol*, vol. 11, no. 4, pp. 297–304, Oct.–Dec. 2018.

can absorb photon energy from only the UV light region; thus, researchers have attempted to enhance ZnO nanoparticles as a visible-light-driven photocatalyst and reduce the band gap by coupling ZnO with conductors such as g-C_3N_4 [6]. Recently, bismuth oxyiodide photocatalyst has gained interest as a coupling semiconductor because of its narrow band gap energy (1.82 eV) [7], [8]. Combined bismuth oxyiodide/titanium dioxide (BiOI/TiO_2) photocatalysts have shown enhanced photocatalytic activities in the visible light region by typical catalytic processes [9]. Thus, BiOI has potential as a composite semiconductor to prepare a BiOI/ZnO heterostructure which could improve absorption activity through 1) reducing the band gap energy required in the visible range, and 2) obtaining an appropriate ratio between BiOI and ZnO for optimal interfacial connection to facilitate transfer of electron-hole pairs [10]. Following the typical method, an aqueous suspension was investigated for photocatalysis. Separation step of the catalyst was applied with loss of photocatalyst amount in the heterogeneous system while under irradiation [11]. To our knowledge, no research has so far been conducted concerning the degradation of methomyl carbonate pesticides over BiOI/ZnO photocatalyst films synthesized under visible light irradiation ($\lambda > 400$ nm). Formation of catalyst film is a promising method to decrease loss of catalyst during reaction interval time as well as reducing filter syringe experimental cost. Moreover, film catalysts are convenient and can be reused as photocatalysts [12].

In this work, BiOI/ZnO heterostructure photocatalyst films were prepared using a simple low temperature co-precipitation method coupled with a reflux procedure. Physicochemical properties of the samples were determined to evaluate results attributed to photoactivity and photocatalytic degradation of aqueous methomyl solution over the as-prepared films was investigated under visible light illumination.

2 Experimental

2.1 *Photocatalyst synthesis*

BiOI/ZnO composite powder was synthesized using a simple low temperature co-precipitation with reflux method. Percentage molar ratio of Bi : Zn was varied as 0.125, 0.25 and 0.50 (denoted as 0.125% BZ, 0.25% BZ and 0.50% BZ). Zinc acetate dihydrate ($Zn(CH_3COO)_2.2H_2O$) was dissolved deionized (DI) water and the solution was slowly dropped into 0.4 M NaOH solution. The mixture was vigorously stirred at 80°C for 2 h when the transparent suspension suddenly turned white. The precipitate was washed several times with 95% ethanol and deionized water and dried at 60°C for 24 h. Synthesized ZnO (pure ZnO) was obtained by calcination at 500°C for 3 h. BiOI/ZnO composite catalysts were subsequently prepared using bismuth nitrate pentahydrate ($Bi(NO_3)_3.5H_2O$) as the bismuth precursor and potassium iodide (KI) as the iodine source. A stoichiometric Bi source solution was mixed with KI solution and continuously stirred at room temperature for 30 min. Then, ZnO suspension was added drop by drop and the pH was adjusted to 7.0. Finally, the suspension was refluxed at 95°C for 3 h under continuous stirring. Pure BiOI was also produced by the same method for comparison purpose.

2.2 *Film preparation*

The photocatalyst film was coated by doctor blading following the protocol used in our previous report [13]. One gram of sample was mixed in 40 µL of glacial acetic acid, then 10 µL Triton X was added as a surfactant and subsequently 0.5 µL of DI water was dropped into the slurry. The mixture was ground and sonicated to disperse the agglomerated particles. Films were annealed at 350°C for 1 h. Finally, catalyst film thicknesses were measured by a Veeco Dektak 6M Stylus Profilometer.

2.3 *Characterization*

X-ray diffraction patterns were obtained using an XRD diffractometer (XRD, PANalytical X'Pert PRO MPD with Cu–K_α radiation, λ = 1.5401 Å) for phase crystalline confirmation. Diffused reflectance UV-vis spectra were recorded by a UV-vis-DRS (Shimadzu UV-3101PC) and the Kubelka-Munk emission function was used to calculate absorption spectra. Morphological structure was determined by field emission scanning electron microscopy with energy dispersive X-ray spectroscopy (FE-SEM-EDS, Hitachi S-4800) and transmission electron microscope (TEM, Hitachi S-4800). Specific surface area (SBET) values were performed by N_2 adsorption (Micromeritics

Tristar 3000). Finally, the oxidation state was obtained using X-ray photoelectron spectroscopy (XPS, PHOIBOS 100 Al, K_α radiation). Peaks in XPS spectra were calibrated with the C 1s peak at 285 eV.

2.4 *Photocatalytic studies*

Photocatalyst film was laid in a cylindrical reservoir containing 20 mg/L of methomyl solution. A 50 W halogen lamp with light density of 340 m^2/W was utilized. A cut-off filter was used to remove photons with $\lambda < 400$ nm. Before turning the light on, the dark adsorption was established for 30 min to obtain adsorption-desorption equilibrium. After illumination, 4 mL of clear solution was withdrawn at interval time of 30 min to measure the absorption spectra of methomyl (λ_{max} = 234 nm) by a T92+ PG Instrument UV-vis spectrophotometer [14].

3 Results and Discussion

3.1 *X-rays diffraction patterns*

Figure 1 shows the XRD patterns of BiOI/ZnO composite photocatalysts compared to pure BiOI and pure ZnO. Peaks of pure BiOI at 29.6º, 31.6º, 37.0º, 39.3º and 45.3º of tetragonal BiOI correspond to (012), (110), (013), (014) and (112) crystal planes of tetragonal structure in agreement with JCPDS file no.10-0445 [15]. Diffraction peaks of pure ZnO at 2θ of 31.7º, 34.4º, 36.3º, 47.5º, 56.6º and 62.9º can be assigned to (100), (002), (101), (102), (110), and (103) crystal planes of hexagonal wurtzite ZnO (JCPDS file no. 36-1451) [16]. XRD patterns of all BiOI/ZnO composites exhibit characteristic peaks of both pure BiOI and ZnO crystalline phases. Using the strongest peaks of ZnO (101) and BiOI (012) planes, average crystallite sizes of BiOI and ZnO, determined by the Scherrer equation [Equation (1)], can be obtained as shown in Table 1 [17].

$$L = 0.9\,\lambda/\beta\,(\cos\theta) \tag{1}$$

where λ is the wavelength of the X-ray in Angstrom (1.541), β is full width at half maximum in radians, θ is the angle between the incident and diffracted beams in degrees and L is an average crystallite size of the sample in nm. Brunauer-Emmett-Teller surface area

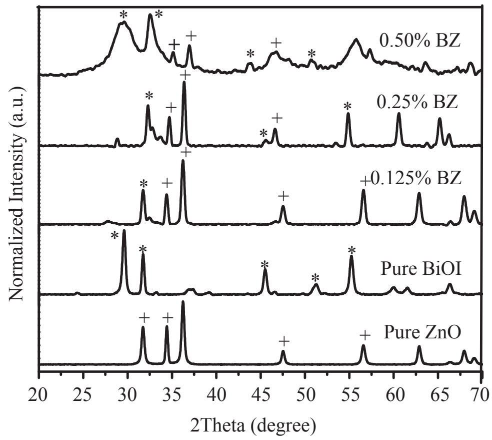

Figure 1: XRD Patterns of as-prepared photocatalyst films with varying molar ratios.

(S_{BET}), pore size diameter and pore volume of as-synthesized samples are shown in Table 1. As clearly seen in Figure 1 and Table 1, diffraction peaks of BiOI become broader and shift toward the lower angles when BiOI content in BiOI/ZnO composites increased. Tetragonal BiOI might penetrate into the hexagonal wurtzite ZnO crystal structure and influence crystal growth-induced collapse [18]. This result can be seen from the XRD pattern of 0.5% BZ, suggesting the smallest average crystallite size compared to the other samples. In addition, good crystallinity of the heterostructure catalyst is needed to achieve crystallization of the pore walls; thus, for photocatalytic application, crystalline ZnO is much preferred [19], [20]. High content of BiOI was the major reason for changed crystal structure of the heterojunction BiOI/ZnO. However, loading high BiOI content into the ZnO component gave values of SBET, pore sizes diameter and pore volumes significantly higher than pure ZnO and BiOI. This suggested that more molecules of methomyl were adsorbed on the catalyst surface leading to beneficial factors of enhanced photocatalytic activity [21].

Table 1: Average crystallite size, SBET, pore size diameter and pore volume of as-synthesized samples

Sample	Average Crystallite Size (nm)	S_{BET} (m^2/g)	Pore Size Diameter (nm)	Pore Volume (cm^3/g)
Pure BiOI	15.55	15.55	33.18	0.139
Pure ZnO	37.07	25.60	35.47	0.227
0.125% BZ	41.42	31.09	37.83	0.284
0.25% BZ	32.40	35.65	38.37	0.302
0.50% BZ	23.28	42.10	41.62	0.363

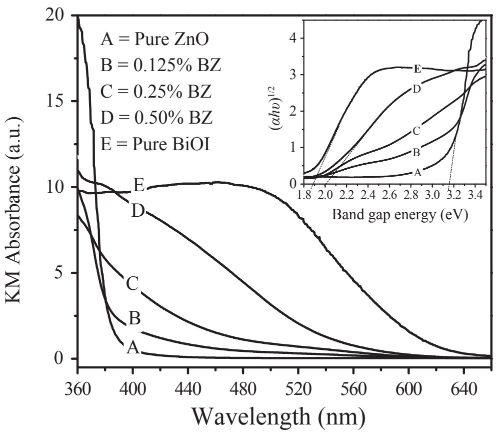

Figure 2: DR-UV-Vis Absorption spectra inset of band gap energies of prepared photocatalyst.

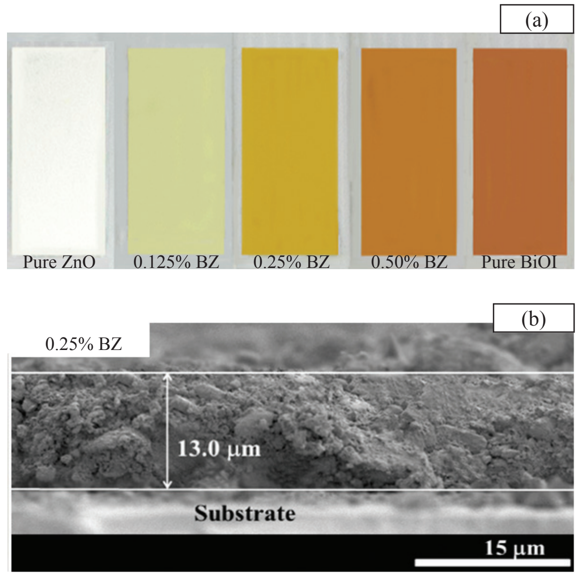

Figure 3: (a) Appearance of photocatalyst samples film and (b) thickness of 0.25% BZ composite film.

3.2 *DR-UV-vis spectra results*

As seen from Figure 2, pure ZnO has spectrum onset of 384 nm, with pure BiOI as ~610 nm corresponding to band gap energy of ~1.84 eV. Photocatalysts were observed at 0.125, 0.25 and 0.5 mol% corresponding to ~2.05, ~1.95 and ~1.92 eV, respectively (inset in Figure 2).

The narrowed-band-gap of prepared photocatalyst samples required less photon energy to improve absorption harvesting under the visible light region. These results suggested that as-synthesized composite samples were able to generate electron-hole pairs under visible light irradiation which further enhanced photocatalytic degradation of methomyl solution.

3.3 *Morphology and microstructure*

The appearance and color of photocatalyst films change from pale white to light brown as BiOI increases from 0.125 to 0.50 mol% in the composite samples [Figure 3(a)]. FE-SEM micrographs of 0.25% BZ samples exhibit thickness of ~13 μm [Figure 3(b)] measured by a profilometer. Thicknesses of pure ZnO, pure BiOI, 0.125% BZ, 0.25% BZ and 0.50% BZ films were 13.03, 12.98, 13.02, 13.00, 12.98 and 13.02 μm, respectively. SEM-EDX and TEM analytical techniques were employed for morphology and microstructure, element composition and particle size of synthesized samples. Images of pure ZnO and pure BiOI are displayed in Figure 4. Pure ZnO has a plate-like shape with BiOI showing a rod-like structure. In addition, 0.25% BZ exhibits a rod-like shape of ZnO particles penetrated into BiOI sheet in the composite sample, with agglomerated large sizes in the range of 100–200 nm. TEM images of ZnO, BiOI, 0.25% BZ and HR-TEM of composite samples are exhibited in Figure 4(c), (d), (f) and (g), respectively. ZnO displays rod-like shape with diameter ~40 nm while BiOI has a 2D plate-like lamella structure with average diameter in the range of 25–40 nm. Rod-like ZnO are embedded in the plate-like structure of BiOI in the composite sample [Figure 4(f)], while Figure 4(g) exhibits the interfacial connection between BiOI and ZnO nanoparticles with lattice spacing of 0.30 nm that corresponded well with (102) tetragonal BiOI plane, (101) crystal plane of wurtzite ZnO, and 0.28 nm of BiOI [22]. This result is consistent with XRD analysis. Moreover, EDX spectra confirmed the existence of Bi, O, I and Zn elements composed in the composite photocatalyst.

3.4 *XPS Analysis*

Oxidation states and surface chemical compositions were examined by XPS. Figure 5(a) shows Bi^{3+} composed in the survey spectra of 0.25% BZ, pure

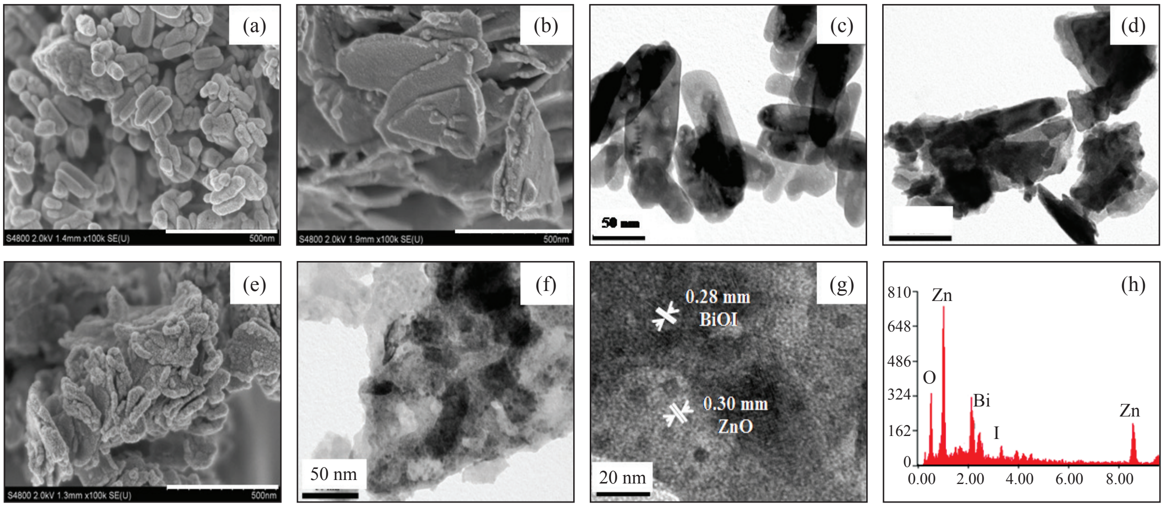

Figure 4: (a), (c) SEM and TEM micrographs of pure ZnO, (b,d) SEM and TEM micrographs of pure BiOI (e), (f) SEM and TEM images of 0.25% BZ sample, (g) HR-TEM with lattice fringe of 0.25% BZ and (h) EDS of 0.25% BZ sample.

BiOI and ZnO, respectively. Composite samples were composed of Bi, O, I, C and Zn elements. Figure 4(e) shows the binding energies of *ca*. 618.5 eV (I $3d_{3/2}$) and 630.5 eV (I $3d_{5/2}$) in agreement with BiOI [23]. For all spectra of composite films, peaks shifted to higher wavelength in comparison to pure ZnO. This implied consolidation of BiOI and ZnO catalysts due to electron transformation in the process of photocatalysis as chemical interaction [24]. The O 1s spectrum [Figure 5(d)] of composite sample can be fitted into 3 peaks with binding energies of 529.5, 531.5 and 532.5 eV ascribed to O-H surface hydroxyls from water, Zn-O bond, and Bi-O chemical bond from the sample of 0.25 mol% nanocomposite [25], respectively. The I3d core level is consistent with the EDS spectrum. The C1s peak at 284.8 eV might occur from hydrocarbon calibration in the XPS instrument. Binding energies of 1021.5 and 1044.5 eV can be indexed to Zn $2p_{3/2}$ and Zn $2p_{1/2}$, respectively. This evidence could be attributed to Zn^{2+} in pure ZnO [Figure 5(b)] [26]. Peaks in Figure 5(c) at 159.2 eV and 164.5 eV are for Bi $4f_{7/2}$ and Bi $4f_{5/2}$, respectively. This XPS analysis shows that n-type ZnO nanorods are deposited on p-type BiOI nanosheets and electrons in ZnO diffuse to BiOI forming p-n heterojunctions; thus, in the space charge region, ZnO is positively charged which increases the binding energy of electrons in Ti 2p chemical states [27].

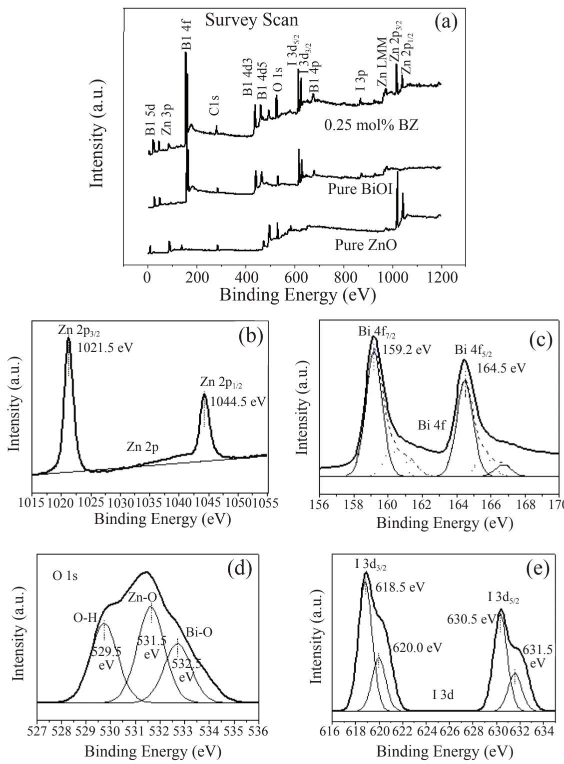

Figure 5: (a) XPS survey scan of pure ZnO, pure BiOI, 0.25% BZ, (b) XPS spectra of Zn 2p, (c) Bi 4f, (d) O1s, and (e) I 3d of 0.25% BZ photocatalyst film, respectively.

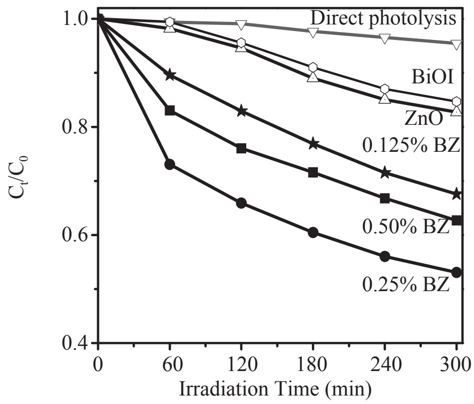

Figure 6: Photocatalytic activities of obtained catalyst films for methomyl degradation under visible light irradiation.

3.5 *Photocatalytic activity*

Photocatalytic activity was evaluated by decomposition of aqueous methomyl insecticide over the entire photocatalyst films under visible light irradiation. Commercial ZnO film and direct photolysis were also investigated for comparison. Figure 6 shows that enhanced BiOI/ZnO composite photocatalyst films reveal ~3 times higher activities than pristine ZnO and commercial ZnO. The UV-vis DRS results clearly suggest that the heterojunction of the BiOI/ZnO sample influences and encourages photocatalytic performance due to a shift of the ZnO band gap toward the visible light region. Composite films showed a decrease of ZnO band gap energy with increased BiOI content, concurring with DR UV-vis results in Figure 2. However, physiochemical properties of the obtained photocatalysts such as phase composition, surface area, pore volume and morphology can also affect their photocatalytic behaviors, and this should not be neglected [28]. As discussed above, our results suggested 0.25% BZ as the optimal photocatalyst. These films exhibited highest photocatalytic activity under visible light irradiation (58%) with good crystallinity and phase composition between BiOI and ZnO as seen from the XRD pattern, increase of surface area, together with appropriated pore size and pore volume [29].

Moreover, simultaneous aggregation of two semiconductors and interfacial connection between BiOI and ZnO in the composite material, as clearly observed from SEM and TEM results, also influence higher electron-hole transfer. Thus, more electrons are easily transferred, and more •OH radicals are generated [30], resulting in enhancement of photocatalytic efficiency as seen from Figure 6. However, as BiOI content further increased to 0.5 mol%, low phase crystallinity was observed from the XRD results, with relatively lower photocatalytic activity than 0.25% BZ catalyst. In addition, 0.125% BZ exhibited less photocatalytic activity as a result of the wider band gap energy compared to the optimal photocatalyst film.

4 Conclusions

BiOI/ZnO composite photocatalyst films were successfully prepared using a simple low temperature co-precipitation method coupled with reflux and doctor blading. Increase in photodegradation activities was shown by all composite photocatalyst films with 0.25 mol% BiOI/ZnO recording the highest photocatalytic performance in comparison with pure ZnO, pure BiOI and commercial ZnO. Narrowed band gap energy caused high absorption of photons from the visible light region, while strong crystalline structure with high SBET values and good arrangement of morphological structure and chemical composition of the catalyst all enhanced methomyl insecticide photocatalytic removal efficiency.

Acknowledgments

The author would like to thank Uttaradit Rajabhat University for financial support (Grant-GOV-URU-02-60), and also acknowledge Dr Ruengwit Sawangkeaw of Institute of Biotechnology and Genetic Engineering, Chulalongkorn University for XPS assistance and Mr Chaiyuth Sae-kung for the film thickness measuring (ARC Centre of Excellence for Electromaterials Science, University of Wollongong, Australia).

References

[1] P. Panuwet, W. Siriwong, T. Prapamontol, R. Nancy, F. Mark, and B. B. Dana, "Agricultural pesticide management in Thailand: Situation and population health risk," *Environmental Science & Policy*, vol. 17, pp. 72–81, Mar. 2012.

[2] S. Kim, H. Ngo, H. Shon, and S. Vigneswaran, "Adsorption and photocatalysis kinetics of

herbicide onto titanium oxide and powdered activated carbon," *Separation and Purification Technology*, vol. 58, pp. 335–342, Jan. 2008.

[3] N. Daneshvar, S. Aber, M. Seyed, M. Dorraji, A. Khataee, and M. Rasoulifard, "Advances in water treatment and pollution prevention," *Separation and Purification Technology*, vol. 56, pp. 58–91, May 2012.

[4] K. Pelentridou, E. Stathatos, H. Karasali, and P. Liano, "Photodegradation of the herbicide using nanocrystalline titania film as photocatalyst and low density black light irradiation or simulated solar excitation source," *Journal of Hazardous Materials*, vol. 163, pp. 756–760, Apr. 2009.

[5] I. Fatimah, S. Wang, F. Xu, W. Feng, and D. Wulandari, "ZnO/montmorillonite for photocatalytic and photochemical degradation of methylene blue," *Applied Clay Science*, vol. 53, pp. 553–560, Oct. 2011.

[6] Z. You, C. Wu, Q. Shen, Y. Yu, H. Chen, Y. Su, H. Wang, C. Wu, F. Zhang, and H. Yan, "A novel efficient g-C_3N_4/BiOI p-n heterojunction photocatalyst constructed through the assembly of g-C_3N_4 nanoparticles," *Dalton Transactions*, vol. 47, pp. 7353–7361, Apr. 2018.

[7] J. Cao, B. Xu, H. Lin, B. Luo, and S. Chen, "Chemical etching preparation of BiOI/BiOBr heterostructures with enhanced photocatalytic properties for organic dye removal," *Chemical Engineering Journal*, vol. 185, pp. 91–99, Mar. 2012.

[8] Y. Long, Y. Wang, D. Zhang, P. Ju, and Y. Sun, "Facile synthesis of BiOI in hierarchical nanostructure preparation and its photocatalytic application to organic dye removal and biocidal effect of bacteria," *Journal of Colloid and Interface Science*, vol. 481, pp. 47–56, Nov. 2016.

[9] B. Li, X. Chen, T. Zhang, S. Jiang, X. Ma, L. Wei, C. Zhao, and W. Chen, "Photocatalytic selective hydroxylation of phenol to dihydroxybenzene by BiOI/TiO_2 p-n heterojunction photocatalysts for enhanced photocatalytic activity," *Applied Surface Science*, vol. 439, pp. 1047–1056, May 2018.

[10] J. Luo, X. Zhou, L. Ma, and X. Xu, "Enhanced visible-light-driven photocatalytic activity of WO_3/BiOI heterojunction photocatalysts," *Journal of Molecular Catalysis A: Chemical*, vol. 410, pp. 168–176, Dec. 2015.

[11] S. Wang, Y. Guan, L. Wang, W. Zhao, C. Sun W. Li, and H. He, "Fabrication of a novel bifunctional material of BiOI/Ag3VO4 with high adsorption-photocatalysis for efficient treatment of dye wastewater," *Applied Catalysis B: Environmental*, vol. 168, pp. 448–457, Jun. 2015.

[12] A. Di, Mauro, M. E. Fragala, V. Privitera, and G. Impellizzeri, "ZnO for application in photocatalysis: From thin films to nanostructures," *Materials Science in Semiconductor Processing*, vol. 69, pp. 44–51, Oct. 2017.

[13] N. Boonprakob, N. Wetchakun, S. Phanichphant, D. Waxler, A. Natasstrad, P. Sherell, J. Chen, and B. Inceesungvorn, "Enhanced visible-light photocatalytic activity of g-C_3N_4/TiO_2 films," *Journal of Colloid and Interface Science*, vol. 417, pp. 402–409, Mar. 2014.

[14] C. Chang, Zhu, Y. Fu, and X. Chu, "Highly active Bi/BiOI composite synthesized by one-step reaction and its capacity to degrade bisphenol A under simulated solar light irradiation," *Chemical Engineering Journal*, vol. 233, pp. 305–314, Nov. 2013.

[15] S. Duo, Y. Li, H. Zhang, T. Liu, K. Wu, and Z. Li, "A facile salicylic acid assisted hydrothermal synthesis of different flower-like ZnO hierarchical architectures with optical and concentration-dependent photocatalytic properties," *Materials Characterization*, vol. 114, pp. 185–196, Apr. 2016.

[16] J. Jiang, H. Wang, X. Chen, S. Li, and Y. Lin, "Enhanced photocatalytic degradation of phenol and photogenerated charges transfer property over BiOI-loaded ZnO composites," *Journal of Colloid and Interface Science*, vol. 494, pp. 130–138, May 2017.

[17] P. Pongwan, B. Inceesungvorn, K. Wetchakun, S. Phanichphant, and N. Wetchakun, "Highly efficient visible-light-induced photocatalytic activity of Fe-doped TiO_2 nanoparticles," *Engineering Journal*, vol. 16, pp. 143–151, Jul. 2012.

[18] Y. Sun, L. Chen, Y. Bao, Y. Zhang, J. Wang, M. Fu, J. Wu, and D. Ye, "The applications of morphology controlled ZnO in catalysis," *Catalysts*, vol. 6, pp. 120–178, Dec. 2016.

[19] C. Chang, H. Yang, N. Gao, and S. Lu, "Core/shell p-BiOI/n-β-Bi_2O_3 heterojunction array with

significantly enhanced photoelectrochemical water splitting efficiency," *Journal of Alloys and Compounds*, vol.738, pp. 138–144, Mar. 2018.

[20] H. Sohrabpoor, E. Aldosari, and N. Gorji, "Modeling the PbI_2 formation in perovskite solar cells using XRD/XPS patterns," *Superlattices and Microstructures*, vol. 97, pp. 556–561, Sep. 2016.

[21] D. Feng, Y. Cheng, J. He, L. Zheng, D. Shao, W. Wang, W. Wang, F. Lu, H. Dong, H. Liu, R. Zheng, and H. Liu, "Enhanced photocatalytic activities of g-C_3N_4 with large specific surface area via a facile one-step synthesis process," *Carbon*, vol. 125, pp. 454–463, Dec. 2017.

[22] T. He, D. Wu, and Y. Tan, "Fabrication of BiOI/$BiVO_4$ heterojunction with efficient visible-light-induced photocatalytic activity," *Materials Letters*, vol. 165, pp. 227–230, Feb. 2016.

[23] W. Liu, M. Wang, C. Xy, S. Chen, and X. Fu, "Synthesis, structural and optical properties of nanoparticles (Al, V) co-doped zinc oxide," *Bulletin of Materials Science*, vol. 39, pp. 7–15, Sep. 2016.

[24] N. Boonprakob, W. Chomkitichai, J. Ketwaraporn, A. Wanaek, B. Inceesungvorn, and S. Phanichphant, "Photocatalytic degradation of phenol over highly visible-light active BiOI/TiO_2 nanocomposite photocatalyst," *Engineering Journal*, vol. 21, pp. 82–91, Jan. 2017.

[25] J. Luo, X. Zhou, L. Ma, and X. Xu, "Enhanced visible-light-driven photocatalytic activity of WO_3/BiOI heterojunction photocatalysts," *Journal of Molecular Catalysis A: Chemical*, vol. 410, pp. 168–176, Dec. 2015.

[26] A. Di, Mauro, M. E. Fragala, V. Privitera, and G. Impellizzeri, "ZnO for application in photocatalysis: From thin films to nanostructures," *Materials Science in Semiconductor Processing*, vol. 69, pp. 44–51, Oct. 2017.

[27] Y. Li, J. Wang, B. Liu, L. Dang, H. Yao, and Z. Li, "BiOI-sensitized TiO_2 in phenol degradation: A novel efficient semiconductor sensitizer," *Chemical Physics Letters*, vol. 508, pp. 102–106, Oct. 2011.

[28] H. Cheng, J. Wang, Y. Zhao, and X. Han, "Effect of phase composition, morphology, and specific surface area on the photocatalytic activity of TiO_2 nanomaterials," *RSC Advances*, vol. 4, pp. 47031–47038, Sep. 2014.

[29] S. Dong, J. Sun, Y. Li, C. Yu, Y. Li, and J. Sun, "Applied $ZnSnO_3$ hollow nanospheres/reduced graphene oxide nanocomposites as high-performance photocatalysts for degradation of- metronidazole," *Applied Catalysis B: Environmental*, vol. 144, pp. 386–393, Jan. 2014.

[30] Y. Li, J. Wang, B. Liu, L. Dang, H. Yao, and Z. Li, "BiOI-sensitized TiO_2 in phenol degradation: A novel efficient semiconductor sensitizer," *Chemical Physics Letters*, vol. 508, pp. 102–106, Oct. 2011.